Incorporating pulse wave velocity into model-based pulse contour analysis method for estimation of cardiac stroke volume

Rachel Smith[a,*], Joel Balmer[a], Christopher G. Pretty[a], Tashana Mehta-Wilson[a], Thomas Desaive[b], Geoffrey M. Shaw[c], J. Geoffrey Chase[a]

[a] *Department of Mechanical Engineering, University of Canterbury, New Zealand*

[b] *IGA Cardiovascular Science, University of Liège, Liège, Belgium*

[c] *Christchurch Hospital Intensive Care Unit*

[*] Corresponding Author
Email address: rachel.smith@pg.canterbury.ac.nz (Rachel Smith)

Preprint submitted to Computer Methods and Programs in Biomedicine April 30, 2020

Abstract

Background and Objectives: Stroke volume (SV) and cardiac output (CO) are important metrics for hemodynamic management of critically ill patients. Clinically available devices to continuously monitor these metrics are invasive, and less invasive methods perform poorly during hemodynamic instability. Pulse wave velocity (PWV) could potentially improve estimation of SV and CO by providing information on changing vascular tone. This study investigates whether using PWV for parameter identification of a model-based pulse contour analysis method improves SV estimation accuracy.

Methods: Three implementations of a 3-element windkessel pulse contour analysis model are compared: constant-Z, water hammer, and Bramwell-Hill methods. Each implementation identifies the characteristic impedance parameter (Z) differently. The first method identifies Z statically and does not use PWV, and the latter two methods use PWV to dynamically update Z. Accuracy of SV estimation is tested in an animal trial, where interventions induce severe hemodynamic changes in 5 pigs. Model-predicted SV is compared to SV measured using an aortic flow probe.

Results: SV percentage error had median bias and [(IQR); (2.5th, 97.5th percentiles)] of -0.5% [(-6.1%, 4.7%); (-50.3%, +24.1%)] for the constant-Z method, 0.6% [(-4.9%, 6.2%); (-43.4%, +29.3%)] for the water hammer method, and 0.8% [(-6.5, 8.6); (-37.1%, +47.6%)] for the Bramwell-Hill method.

Conclusion: Incorporating PWV for dynamic Z parameter identification through either the Bramwell-Hill equation or the water hammer equation does not appreciably improve the 3-element windkessel pulse contour analysis model's prediction of SV during hemodynamic changes compared to the constant-Z method.

Keywords: Pulse contour analysis, Pressure contour analysis, Pulse wave velocity, Windkessel model, Stroke volume, Cardiac output, Hemodynamic monitoring, Intensive care

1. Introduction

Circulatory failure occurs in around 30% of patients admitted to an intensive care unit (ICU) [1] and is a major contributor to ICU mortality [2]. Thus, hemodynamic monitoring is a fundamental part of managing critically ill patients. Cardiac output (CO) and stroke volume (SV) are useful clinical metrics for diagnosing and managing circulatory failure [3, 4, 5, 6], providing information on blood flow out of the heart on average and beat-by-beat, respectively. The European Society of Intensive Care Medicine has recommended using CO and SV measured in real-time to evaluate patient status and response to therapy [7].

However, CO and SV are not readily measurable clinically. The clinical gold standard monitoring method for CO, indicator dilution, is invasive and intensive [6, 8]. Non-additionally invasive pulse contour analysis methods use only an arterial waveform to estimate CO. However, current clinically available non-additionally invasive devices have insufficient accuracy for use in critically ill patients [8]. Further work is needed to develop non-additionally invasive monitoring for CO or SV, which is reproducible and reliable across a range of physiological states [9].

A recent experimental pulse contour analysis model [10] uses common clinical measures as inputs to a 3-element windkessel model to estimate beat-to-beat SV with clinically acceptable accuracy. Using pulse wave velocity (PWV) for parameter identification of this model could potentially improve SV estimates because PWV provides information on the vascular tone / stiffness

of the arteries, which affect how SV is calculated from pressure [11, 12]. A prior model by some authors [13] improved SV estimation accuracy by using PWV introduced via both the Bramwell-Hill and water hammer equations. However, while accurate, it delivered non-physiological flow waveforms to calculate SV due to difficulty with parameter identification, an issue resolved in the more recent model [10].

This study aims to test whether introducing PWV for dynamic parameter identification of the recent model in [10] provides an improved estimate of stroke volume during hemodynamic instability. The model is tested on pigs undergoing hemodynamic interventions which cause rapid changes in SV and PWV, and represents a novel approach to improving non-additionally-invasive, beat-to-beat model-based SV estimation. Accurate beat-to-beat estimation of SV would enable direct monitoring of heart function and response to care with insight and resolution not currently possible.

2. Methods

2.1. Porcine Trials and Measurements

Data are from 5 pure Piétrain pigs, weighing 18.5 kg to 29.0 kg. Pigs were initially sedated and anesthetized using Zoletil ($0.1\,\mathrm{mL\,kg^{-1}}$) and diazepam ($1\,\mathrm{mg\,kg^{-1}}$). Sedation and anesthesia was maintained via a continuous infusion of sufentanil ($0.1\,\mathrm{mL\,kg^{-1}\,h^{-1}}$ at $0.005\,\mathrm{mg\,mL^{-1}}$), Thiobarbital ($0.1\,\mathrm{mL\,kg^{-1}\,h^{-1}}$) and Nimbex ($1\,\mathrm{mL\,kg^{-1}\,h^{-1}}$ at $2\,\mathrm{mg\,mL^{-1}}$), delivered via a superior vena cava catheter. Pigs were mechanically ventilated via a tracheostomy, using a GE Engstrom CareStation mechanical ventilator (GE 92 Healthcare, Waukesha, US) with baseline positive end-expiratory pressure (PEEP) of 5 $\mathrm{cmH_2O}$ and tidal volume of $10\,\mathrm{mL\,kg^{-1}}$.

Blood pressure was measured using high fidelity pressure catheters (Transonic, Ithaca, NY, USA) in the proximal aorta (P_{ao}), femoral artery (P_{mea}), and vena cava (P_{cvp}). Left ventricular pressures and volumes (V_{LV}) were measured using 7F micromanometer-tipped admittance catheters (Transonic Scisense Inc., Ontario, Canada). Flow into the aorta (Q_{ao}) was measured using an aortic flow probe positioned on the proximal aorta, near to the aortic valve (Transonic, Ithaca, NY, USA). Once the probe was located, the thorax was held closed using clamps. All data was measured with a sampling rate of 250 Hz, and recorded as a single Notocord data file (Instem, Croissy-sur-Seine, France).

Pigs underwent a series of hemodynamic interventions:

- A respiratory recruitment manouevre in which PEEP is increased in steps of 5 cmH_2O. Increasing PEEP reduces systemic venous return to the right heart and increases pulmonary resistance. The reduction in flow in and out of the right ventricle leads to a corresponding drop in flow into the left ventricle and a drop in SV [5, 14]. The effect of PEEP changes may be reduced due to the opening and then clamping of the chest for placement of the aortic flow probe.

- An infusion of saline solution (500 mL over 30 min, prior to the endotoxin infusion). This intervention aims to increase circulatory volume and ventricular preload. Data from during the infusion was not used in this study.

- An infusion of endotoxin ($0.5\,mg\,kg^{-1}$ of E. Coli lipopolysaccharide over 30 minute) to produce a septic shock like response: inflammation, capillary leakage, decreased afterload, hypovolemia, tissue hypoxia and eventual cardiac failure [15, 16].

2.2. Ethics

Pig experiments were conducted at the Centre Hospitalier Universitaire de Liège, Belgium and were approved by the Ethics Committee of the University of Liège Medical Faculty, permit number: 14-1726.

2.3. Data Collection

From each pig experiment, two interventions were identified and analysed:

1. *Recruitment Manoeuvre:* 8 minutes encompassing a recruitment manoeuvre, prior to fluid and endotoxin infusions.
2. *Endotoxin:* In Pigs 2 and 4 this stage is the final 8 minutes of the 30 minute endotoxin infusion. Pigs 1, 3, and 5 responded dramatically to the endotoxin, with pressure measures dropping so low as to suggest circulatory failure before completion of the 30 minutes. In these pigs, the endotoxin stage is 8 minutes up until circulatory failure.

These interventions led to large changes in SV for most pigs, providing a good test for whether the model can track SV during unstable hemodynamic states. The fluid infusion intervention is not used as SV remained stable.

The experimental time-schedule is illustrated in Fig 1. The first 10 beats of each intervention are used for model calibration. All subsequent beats in the interventions are used to test the ability of the model to track SV changes in response to the interventions. Across the 5 pigs, each with 2 interventions, there were a total of 5531 beats.

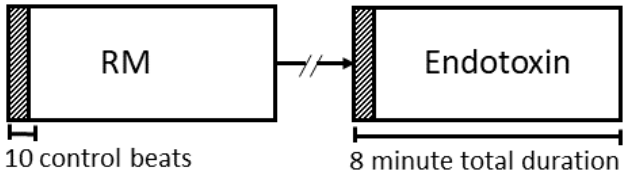

Figure 1: Schematic representation of data collected for each pig. Two 8-minute interventions are used. The first 10 beats of each intervention are used as a control period for calibration of the model.

2.4. Pulse contour analysis method

The 3-element windkessel model of the cardiovascular system, shown in Fig 2, relates pressure and flow in the large arteries [17, 18, 19]. The model lumps the spatially varying properties of the arteries into three parameters: characteristic impedance (Z) represents resistance to flow into the windkessel / reservoir; reservoir compliance (C); and resistance (R) to flow leaving the reservoir and and emptying into the venous system [17, 18]. The downstream pressure of the venous system is assumed to be constant for a given beat, and equal to the average central venous pressure during that beat, $\overline{P}_{cvp}$.

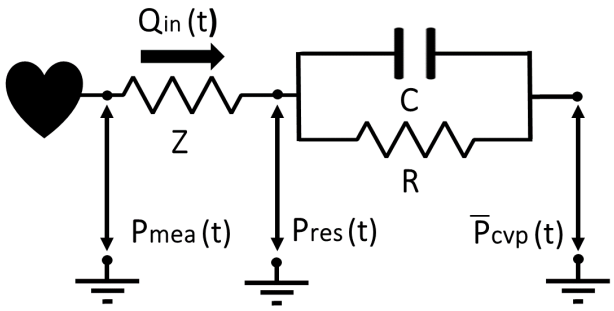

Figure 2: Schematic representation of the 3-element windkessel model of the arterial system. P_{mea} is a measured arterial pressure waveform, P_{res} is the modelled reservoir pressure, and $\overline{P}_{cvp}$ is the downstream pressure. Q_{in} is flow into the reservoir.

The model uses a measured arterial pressure waveform (P_{mea}), in this case from the femoral artery, as an input. The model divides P_{mea} into a reservoir pressure component (P_{res}) associated with filling of the reservoir, and an excess pressure component (P_{ex}):

$$P_{mea}(t) = P_{ex}(t) + P_{res}(t) \tag{1}$$

P_{ex} is the pressure drop caused by ejecting blood from the ventricle into the reservoir, and is directly proportional to flow into the reservoir (Q_{in}):

$$Q_{in}(t) = \frac{P_{ex}(t)}{Z} \tag{2}$$

Q_{in} is equivalent to flow into the aorta [20], under the assumption this lumped parameter model can adequately describe arterial dynamic properties. Hence, integrating the excess pressure waveform over one beat can be used to estimate SV (SV_{est}):

$$SV_{est,\,n} = \frac{1}{Z} \int_{t_{0,n}}^{t_{0,n+1}} P_{ex}(\tau)\; d\tau \tag{3}$$

where the nth beat begins at the P_{mea} waveform foot $t_{0,n}$ and ends at the subsequent P_{mea} waveform foot $t_{0,n+1}$. The pressure waveform foot, which marks the beginning of systole, is detected using an algorithm presented elsewhere [21].

An example of P_{ao}, P_{mea} and P_{res} waveforms for a single beat are given Fig 3, with the location of t_0 identified.

2.5. Identification of reservoir and excess pressure waveforms

The reservoir pressure waveform (P_{res}) can be calculated from P_{mea} for a given beat if parameter products RC and ZC are known [10]:

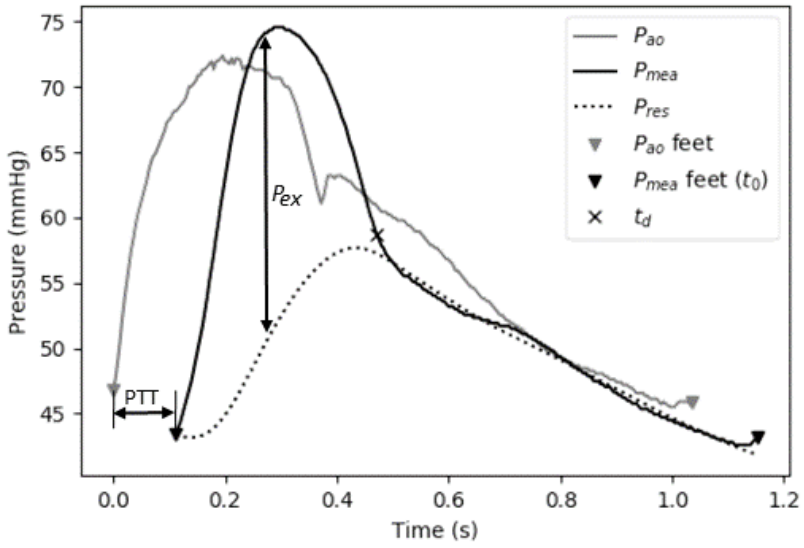

Figure 3: Example of P_{ao}, P_{mea}, and P_{res} for a single beat. PTT is the time difference between the P_{ao} and P_{mea} feet. P_{ex} is the pressure difference between P_{mea} and P_{res}.

$$P_{res}(t) = e^{-(\frac{1}{[ZC]_n}+\frac{1}{[RC]_n})t}\left(\int_{t_{0,n}}^{t_{0,n+1}} e^{(\frac{1}{[ZC]_n}+\frac{1}{[RC]_n})\tau}\left(\frac{P_{mea}(\tau)}{[ZC]_n}+\frac{\overline{P}_{cvp}}{[RC]_n}\right)d\tau + P_{mea}(t_{0,n})\right)$$

$$\text{where } (t_{0,\,n} < t < t_{0,\,n+1}) \tag{4}$$

where RC and ZC values are identified from P_{mea} on a beat-wise basis as an optimization problem [10] by enforcing the condition there is no flow into the aorta during diastole. Thus, $P_{ex} = 0$ in diastole, and Equation 1 yields:

$$P_{res}(t_{d,\,n} < t < t_{0,\,n+1}) = P_{mea}(t_{d,\,n} < t < t_{0,\,n+1}) \tag{5}$$

where $t_{d,n}$ is the beginning of diastole for the nth beat, demonstrated in Fig

3. $t_{d,n}$ is identified using a weighted second derivative algorithm presented elsewhere [22],

Knowing P_{res}, Equation 1 can be used to calculate P_{ex}, and subsequently Q_{in} and beat-to-beat SV via Equations 2 and 3, respectively.

2.6. Identification of Characteristic Impedance Using Pulse Wave Velocity

The remaining model parameter Z must be identified to obtain an an estimate of SV from P_{ex} using Equation 3. Z is a lumped parameter modelling the impedance to flow in the large conduit arteries as a resistance. Three methods to estimate Z are compared in this study.

1. ***constant-Z:*** For each stage, Z is set to a single constant value, $\overline{Z}_{control}$. This method has previously been shown to provide acceptable accuracy for SV estimation [10]. Z is calculated for each of the first 10 beats of a stage through calibration against the validation SV metric (SV_{mea}), obtained from an aortic flow probe, using a rearrangement of Equation 3:

$$Z_{control,\,n} = \frac{1}{SV_{mea,\,n}} \int_{t_{0,n}}^{t_{0,n+1}} P_{ex}(\tau)\, d\tau \tag{6}$$

   Z values for the first 10 beats are then averaged to reduce the impact of measurement noise, obtaining $\overline{Z}_{control}$:

$$\overline{Z}_{control} = \frac{\sum_{k=1}^{10} Z_{control,\,k}}{10} \tag{7}$$

In a clinical setting the model could be calibrated using a non-invasive SV metric such as from echocardiography.

2. ***Water hammer:*** Z can be related to pulse wave velocity using the water hammer equation [17], which assumes a rigid tube with no reflections [23, 24]. PWV is calculated using the the pulse transit time (PTT) between the foot of the P_{ao} and P_{mea} waveforms (Fig 3), where pressure catheter sites are separated by a fixed distance, d, yielding:

$$PWV = \frac{d}{PTT} \tag{8}$$

Hence, the water hammer equation can be used to express Z for a given beat in terms of PTT:

$$Z_{wh,\,n} = \frac{\rho\, d}{A\, PTT_n} \tag{9}$$

where ρ is the density of blood and A is the cross area of the proximal aorta, which are assumed to be constant.

To avoid the need to identify A and d, $Z_{wh,n}$ is calibrated for the first 10 beats of each intervention using $\overline{Z}_{control}$, the baseline calibration factor. $\overline{Z}_{control}$ is obtained by finding the ideal value of Z, such that $SV_{est,cont}$ is equal to SV_{mea} during the 10-beat control period. In order to ensure that $SV_{est,wh}$ is equal to SV_{mea} during control, $Z_{wh,cal}$ is set equal to $\overline{Z}_{control}$ during the control period using Equation (10):

$$Z_{wh,cal,n} = \overline{Z}_{control} \times \frac{Z_{wh,\,n}}{\overline{Z}_{wh,control}} \tag{10}$$

where $\overline{Z}_{wh}$ is the average Z_{wh} value from the first 10 beats:

$$\overline{Z}_{wh,control} = \frac{\sum_{k=1}^{10} Z_{wh,\,k}}{10} \tag{11}$$

Thus, during the 10 control beats, the fraction in Equation (10) is approximately equal to one, and $Z_{wh,cal,n} \approx \overline{Z}_{control}$.

Substituting Equations 9 and 11 into Equation 10 shows $Z_{wh,cal,n}$ can be calculated by updating $\overline{Z}_{control}$ based upon changes in $1/PTT$:

$$Z_{wh,cal,n} = \overline{Z}_{control} \times \frac{\frac{1}{PTT_n}}{\frac{1}{10}\sum_{k=1}^{10} \frac{1}{PTT_k}} \tag{12}$$

Hence, $Z_{wh,cal,n}$ updates $\overline{Z}_{control}$ each beat based on changes in PWV.

3. ***Bramwell-Hill:*** The Bramwell-Hill equation [25] relates pulse wave velocity and compliance for an elastic, thin walled vessel. The area compliance associated with the conduit arteries, C_A, can be determined beat-wise with the Bramwell-Hill equation using PWV (and thus PTT) for each beat:

$$C_{A,\,n} = \frac{A\,PTT_n{}^2}{\rho\,d^2} \tag{13}$$

The volume based compliance of the windkessel model reservoir, C, can be defined as the product of the area compliance C_A and a characteristic length of the conduit arteries L:

$$C_n = C_{A,\,n}\, L \tag{14}$$

Dividing the identified parameter product ZC by C yields Z_{bh} for the nth beat:

$$Z_{bh,\,n} = \frac{[ZC]_n}{C_n} \tag{15}$$

Substituting in expressions for C_n (Equation 14) and subsequently $C_{A,\,n}$ (Equation 13) yields an expression for $Z_{bh,\,n}$ that incorporates PTT:

$$Z_{bh,\,n} = \frac{\rho\, d^2\, [ZC]_n}{A\, L\, {PTT_n}^2} \tag{16}$$

Z_{bh} is calibrated using $Z_{control}$, the baseline calibration factor, in the same manner as for the water hammer equation, avoiding the need to identify A, L and d:

$$Z_{bh,\,cal,\,n} = \overline{Z}_{control} \times \frac{Z_{bh,\,n}}{\overline{Z}_{bh,control}} \tag{17}$$

where:

$$\overline{Z}_{bh,control} = \frac{\sum_{k=1}^{10} Z_{bh,k}}{10} \tag{18}$$

Substituting Equations 16 and 18 into Equation 17 shows $Z_{bh,cal,n}$ can be calculated by updating $\overline{Z}_{control}$ based upon changes in ZC/PTT^2:

$$Z_{bh,cal,n} = \overline{Z}_{control} \times \frac{\frac{[ZC]_n}{{PTT_n}^2}}{\frac{1}{10}\sum_{k=1}^{10} \frac{[ZC]_k}{{PTT_k}^2}} \tag{19}$$

2.7. Validation SV Measure

The SV metric used for validation and calibration (SV_{mea}) was obtained from the aortic flow probe signal (Q_{ao}) in Pigs 2 - 5. Integrating the filtered flow probe signal over a beat was used to obtain SV_{mea}. For Pig 1 an admittance catheter was used to find SV_{mea} because the flow probe measured physiologically unrealistic flows. In this case, SV_{mea} was calculated as the difference between the maximum and minimum ventricle volume (V_{LV}) for each beat. Both the flow probe and admittance catheter signals were filtered with a low-pass Hamming filter with a cut off frequency of 10 Hz, and transition bandwidth of 10 Hz between the cut and pass bands. An example of raw and filtered signals, with illustration of how SV_{mea} is obtained, is given in Appendix A.

The overall process of this pulse contour analysis method is illustrated in Fig 4.

2.8. Analysis

The SV error (mL), percentage error ($error_{\%}$), and error as a percentage of average SV during the first 10 control beats ($error_{\%control}$) was calculated for each beat independently. This process was followed for each pig, during each of the two interventions they were subjected to (excluding the 10 calibration beats). The entire process was repeated for each of the three methods for estimating Z. Figure 1 shows the two interventions and the 10 control beats used each time. There is no analysis of beats in between these periods.

$error_{\%control}$ is useful because its magnitude is relative to SV during baseline state, whereas $error_{\%}$ becomes very high when SVs fall to only a few mL, for which accuracy of within a few mL is not clinically necessary.

The difference between median error is examined by calculating a 95% confidence interval (CI) for the differences in medians for each pair of methods. CI's were generated empirically by using bootstrapping [26]. For each method, 1000 cohorts of the same size as the original sample (N = 5531 beats) were generated using sampling with replacement. The median of each cohort was calculated. The difference between cohort medians of a given pair of methods was calculated, and a 95% confidence interval (CI) for the difference between medians was calculated. Where this CI does not cross zero, differences in medians are statistically significant with $p \leq 0.05$ [26]. Errors across all pigs and interventions are grouped for this analysis.

A 95% CI for the difference in 95% range of each method (95th percentile - 2.5th percentile) was calculated in the same way as for the difference in

medians. The 95% range of each bootstrap cohort was calculated, and the difference between cohort ranges for a given pair of methods was calculated. Where this CI does not cross zero, differences in 95% range are statistically significant with $p \leq 0.05$ [26].

The agreement between SV_{mea} and SV_{est} of each method is assessed using Bland-Altman analysis [27] for $error_{\%}$ and $error_{\%control}$. In this analysis, the median bias has been used as no assumption is made about how error is distributed, and the 95% range of the error is used for the limits of agreement.

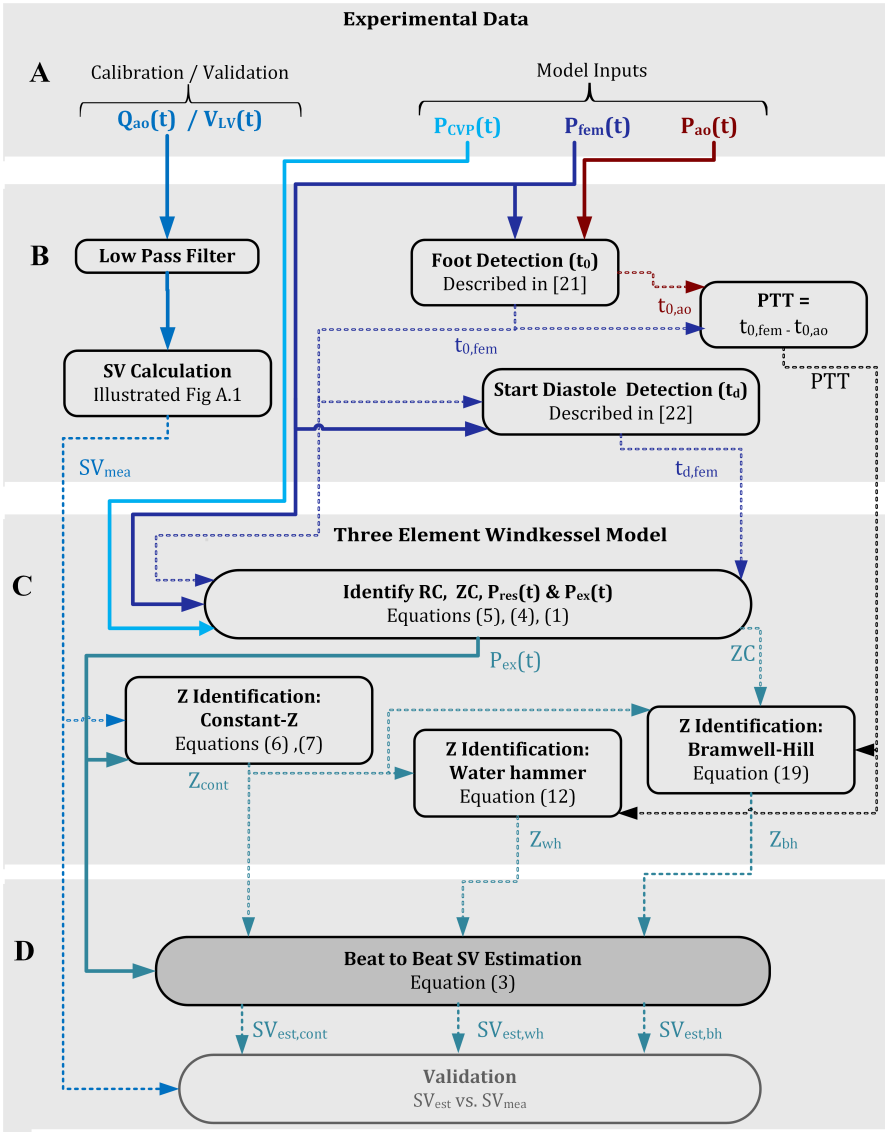

Figure 4: Flow chart for pulse contour analysis method. A) Pressure signals (P_{ao}, P_{fem}, P_{cvp}), Q_{ao}, and V_{LV} are measured in pig experiments. B) Additonal model inputs and validation metrics are calculated. The feet of P_{ao} and P_{mea} are found in order to obtain PTT, and t_d is identified from P_{mea}. SV_{mea} is calculated from Q_{ao} (Pigs 2-5) or V_{LV} (Pig 1). C) Three element windkessel model parameters (ZC, RC), P_{res}, and P_{ex} are calculated beat-wise. Z is calculated in three different ways: set as a constant value (Z_{cont}), using the Water hammer equation (Z_{wh}), and using the Bramwell-Hill equation (Z_{bh}). SV_{mea} during the control period is used to calibrate these methods. D) SV estimates are obtained for each of the three Z methods. SV estimates are compared to SV_{mea} for validation.

3. Results

A summary of the median and range of measured signals (P_{mea}, P_{cvp}, PTT, and SV_{mea}) for each intervention is provided in Table 1. Pig 5 had very low SV_{mea} and P_{mea} mean and pulse pressure (PP) values, suggestive of hypovolemia. Pig 2 had much higher SV_{mea} and P_{mea} mean values compared to all other pigs. During control, SV_{mea} and P_{mea} were stable, with values staying within a small range for all pigs. During the subsequent interventions, a greater range of values were observed.

Table 1: Summary of measured signals for each intervention, all values are presented as median and the 95% range [2.5th percentile, 97.5th percentile]. PP refers to pulse pressure. N is the number of beats. Endo refers to the endotoxin intervention.

	Intervention	N	$\overline{P}_{mea}$	P_{mea} PP	$\overline{P}_{ao}$	P_{ao} PP	$\overline{P}_{cvp}$	PTT	SV_{mea}
			mmHg					s	mL
Pig 1	*RM Control*	10	55 [54 56]	40 [38 40]	59 [58 60]	26 [24 26]	11.9 [11.7, 12.4]	0.108 [0.104, 0.108]	25 [23 28]
	RM	483	50 [29 56]	37 [15 42]	54 [33 60]	25 [15 27]	12.0 [11.5, 15.2]	0.112 [0.104, 0.136]	25 [10 31]
	Endo Control	10	54 [54 55]	32 [31 32]	58 [58 59]	26 [25 26]	12.9 [12.8, 13.2]	0.112 [0.108, 0.116]	26 [24 28]
	Endo	423	53 [30 55]	32 [9, 35]	58 [33 59]	25 [12 26]	12.9 [12.3, 14.0]	0.112 [0.104, 0.142]	24 [12 28]
Pig 2	*RM Control*	10	83 [70 84]	45 [44 58]	72 [60 72]	31 [30 37]	11.3 [10.9, 11.9]	0.092 [0.088, 0.102]	83 [79 90]
	RM	604	82 [74 88]	44 [37 47]	70 [62 76]	29 [20 33]	11.6 [10.5, 13.2]	0.092 [0.084, 0.100]	75 [58 92]
	Endo Control	10	89 [89 89]	43 [42 43]	79 [79 79]	32 [31 32]	9.1 [8.8, 9.8]	0.084 [0.080, 0.088]	66 [64 67]
	Endo	607	88 [86 89]	43 [42 44]	78 [77 80]	31 [29 32]	9.4 [8.7, 10.3]	0.084 [0.080, 0.088]	62 [56 67]
Pig 3	*RM Control*	10	48 [47 49]	32 [30 33]	51 [50 52]	25 [23 25]	5.3 [5.2, 5.4]	0.100 [0.100, 0.108]	39 [37 43]
	RM	605	43 [29 52]	27 [10 35]	45 [33 55]	23 [16 26]	5.6 [5.2, 6.6]	0.104 [0.096, 0.120]	34 [24 42]
	Endo Control	10	46 [46 46]	21 [20 21]	43 [42 43]	19 [19 19]	7.5 [7.4, 7.8]	0.110 [0.108, 0.112]	31 [29 32]
	Endo	547	45 [23 49]	20 [1, 25]	40 [19 44]	17 [8, 19]	8.1 [7.4, 9.6]	0.112 [0.104, 0.153]	26 [6, 32]
Pig 4	*RM Control*	10	43 [43 44]	35 [34 37]	47 [47 48]	23 [22 23]	5.0 [4.8, 5.5]	0.084 [0.081, 0.088]	23 [22 27]
	RM	573	42 [34 46]	34 [23 38]	46 [37 50]	23 [18 25]	5.5 [4.6, 6.4]	0.088 [0.080, 0.096]	23 [18 28]
	Endo Control	10	37 [37 38]	23 [22 23]	38 [38 38]	17 [16 17]	10.7 [10.5, 11.0]	0.092 [0.088, 0.099]	18 [17 19]
	Endo	520	36 [35 38]	21 [19 23]	36 [36 38]	16 [15 17]	8.9 [6.8, 10.7]	0.096 [0.088, 0.104]	17 [15 18]
Pig 5	*RM Control*	10	45 [44 46]	37 [35 38]	51 [50 52]	21 [20 21]	2.9 [2.6, 3.7]	0.096 [0.092, 0.100]	10 [10 10]
	RM	590	38 [26 45]	28 [12 37]	41 [29 50]	17 [10 21]	3.7 [2.6, 5.6]	0.104 [0.092, 0.116]	8 [5, 10]
	Endo Control	10	34 [33 35]	27 [26 28]	37 [37 38]	16 [15 17]	7.9 [7.8, 8.2]	0.110 [0.104, 0.118]	10 [9, 10]
	Endo	579	37 [29 41]	29 [10 31]	41 [24 43]	17 [9, 18]	8.0 [7.5, 10.1]	0.108 [0.096, 0.124]	10 [4, 11]

Fig 5 shows changes in Pig 3's P_{mea}, $1/PTT$, SV_{mea}, and SV_{est} in response to the interventions. Appendix B contains the same plots for all 5 pigs. These Figs show that the RM led to reduced $\overline{P}_{mea}$ and SV_{mea} in Pigs 1,3,4, and 8

but not for Pig 2 which had reduced SV_{mea} without reduction in $\overline{P}_{mea}$. The Endotoxin intervention led to reduced $\overline{P}_{mea}$ and SV_{mea} in Pigs 1,3, and 5. Pigs 2 and 4 were more stable, showing only gradual reduction in SV_{mea} over the course of the intervention.

SV_{est} using each method followed a similar trend over the course of the intervention for Pigs 1, 2, and 4 (Figs B.1, B.2, B.4C). For Pigs 3 and 5 the Bramwell-Hill SV_{est} was very different to that of the Constant-Z and Bramwell-Hill methods (Figs 5, B.5C).

In addition SV changes in response to each intervention, there are also smaller rapid fluctuations in SV (Fig 5 C). These SV variations occur over the course of the respiratory cycle due to cardiopulmonary interactions [28]. Fig 6 gives an example of these SV and P_{mea} fluctuations for the RM intervention.

The median percentage error ($error_{\%}$) for each method, for each pig and stage, is presented in Table 1. Percentage errors for all beats of a given intervention are calculated from the difference between SV_{est} and SV_{mea} signals (which are plotted in Fig 5 C, and in Appendix B).

Table 2: Stroke volume estimation percentage error ($error_{\%}$), presented as median and the 95% range [2.5th percentile, 97.5th percentile] for each pig, intervention, and method

	Recruitment Manouevre			**Endotoxin**		
Pig	constant-Z	Bramwell-Hill	Water hammer	constant-Z	Bramwell-Hill	Water hammer
1	4 [-29, 27]	-6 [-38, 15]	8 [-15, 53]	6 [-39, 34]	3 [-44, 27]	5 [-25, 39]
2	1 [-13, 23]	-2 [-21, 17]	-1 [-16, 21]	-1 [-6, 7]	4 [-7, 16]	0 [-7, 8]
3	-2 [-58, 16]	5 [-12, 36]	-4 [-51, 13]	4 [-85, 32]	-3 [-79, 22]	6 [-83, 29]
4	-5 [-15, 9]	-5 [-21, 22]	-3 [-13, 14]	-2 [-8, 3]	2 [-13, 18]	1 [-8, 9]
5	-4 [-29, 11]	22 [-8, 102]	2 [-19, 19]	3 [-22, 10]	-4 [-25, 92]	2 [-17, 11]

To assess the overall performance of the three methods, the error across all in-

terventions and pigs has been compared, using both $error_{\%}$ and $error_{\%control}$. The distribution of these errors is shown in Fig 7. In all cases, median $error_{\%}$ and $error_{\%control}$ are close to 0, and error is within $\pm$ 30% for at least 90% of beats.

Statistical analysis was used to assess whether the distribution of errors for each method, which are shown in Fig 7, are significantly different. Results from this statistical analysis is provided in Table 3.

The median percentage error was significantly different when comparing the Constant-Z method against both the Water hammer and Bramwell-Hill methods, as the 95% CI for the difference of medians does not cross zero in these cases (Table 3). However, median percentage error was not significantly different between the Water hammer and Bramwell-Hill methods (Table 3).

The 95% range of the errors was significantly larger for the Bramwell-Hill method when compared against both the Constant-Z and water hammer methods. However, 95% range was not significantly different between the Water hammer and Constant-Z methods (Table 3).

Table 3: Results from statistical analysis of differences in percentage errors for each pair of methods. * indicates significant difference ($p \leq 0.05$).

		Difference of medians *95% CI*	**Difference of 95% Range** *95% CI*
Water hammer - Constant-Z	$error_{\%}$	[0.72, 1.39] *	[-6.7, 4.7]
	$error_{\%control}$	[0.70, 1.33] *	[-5.1, 0.0]
Bramwell-Hill - Constant-Z	$error_{\%}$	[0.83, 1.72] *	[2.1, 17.8] *
	$error_{\%control}$	[0.80, 1.60] *	[2.6, 8.2] *
Bramwell-Hill - Water hammer	$error_{\%}$	[-0.28, 0.65]	[3.3, 19.6] *
	$error_{\%control}$	[-0.25, 0.66]	[5.1, 10.3] *

The agreement between SV_{est} and SV_{mea} are shown in the Bland-Altman plots in Figs 8 and 9, which use $error_{\%}$ and $error_{\%control}$ respectively. The x-axis of these plots is the average of SV_{est} and SV_{mea}, and y-axis shows error associated with each SV measurement. When two methods agree well, the data-points are close to zero, and the limits of agreement (2.5th, 97.5th) percentiles are narrow. The Bramwell-Hill method shows the poorest agreement of methods, with the widest limits of agreement, and high errors for Pig 5 in particular. Errors are distributed very similarly for the water hammer and Constant-Z methods.

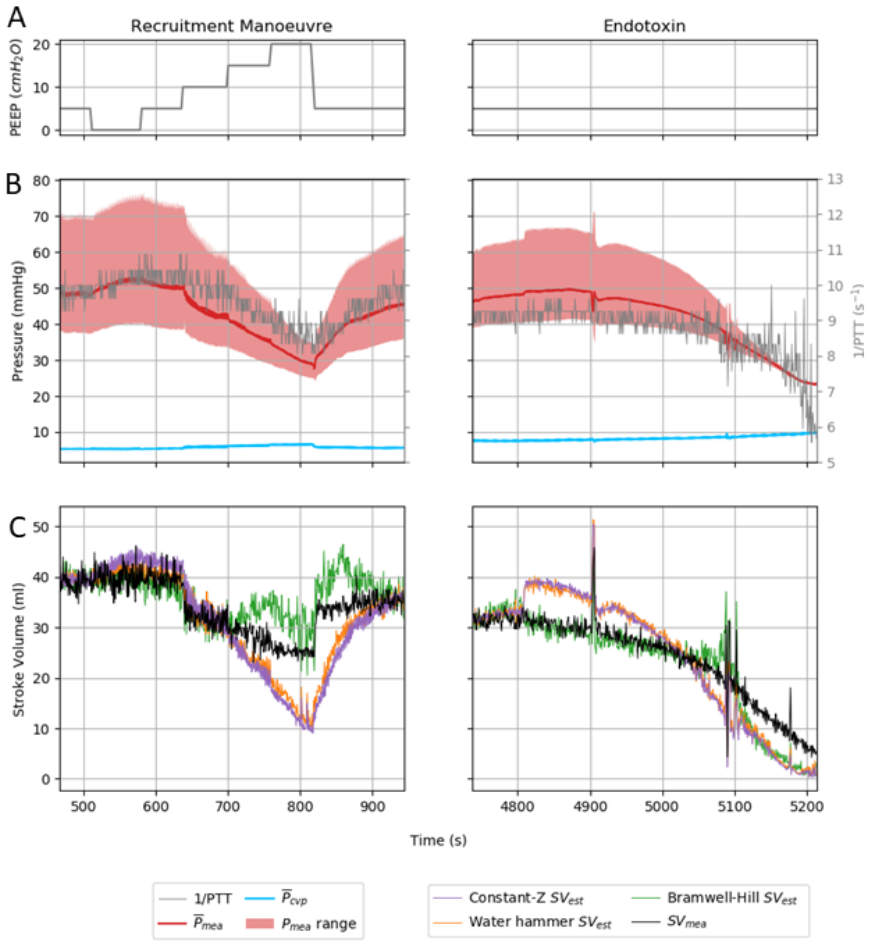

Figure 5: Pig 3 signals for the full duration of both interventions. A) PEEP. For the RM intervention PEEP is increased in steps to induce changes in SV and circulatory pressures. B) Model input signals: P_{cvp} is presented as mean pressure (calculated beat-wise) and P_{mea} is presented as beat-wise mean with the shaded area indicating range of pressures for each beat (foot and maximum pressure). $1/PTT$ is plotted on a secondary y-axis. C) SV_{mea} and modelled stroke volume, SV_{est}, for each method for estimating Z (Constant-Z, Water hammer, Bramwell-Hill)

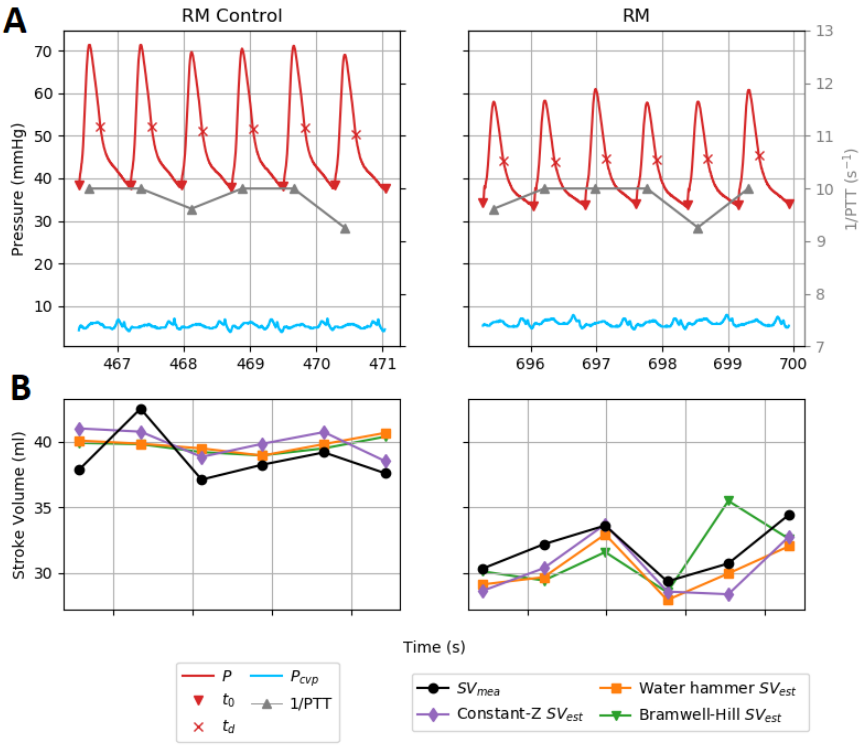

Figure 6: Pig 3 signals for 6 beats during the control period of the RM intervention, and 6 beats in the middle of the RM intervention. A) Model input signals: P_{cvp} and P_{mea} waveforms. The foot (t_0) and beginning of diastole (t_d) for P_{mea} are indicated. $1/PTT$ for each beat is plotted on a secondary y-axis). B) SV_{mea} and modelled stroke volume for each beat, SV_{est}, for each method (Constant-Z, Water hammer, Bramwell-Hill)

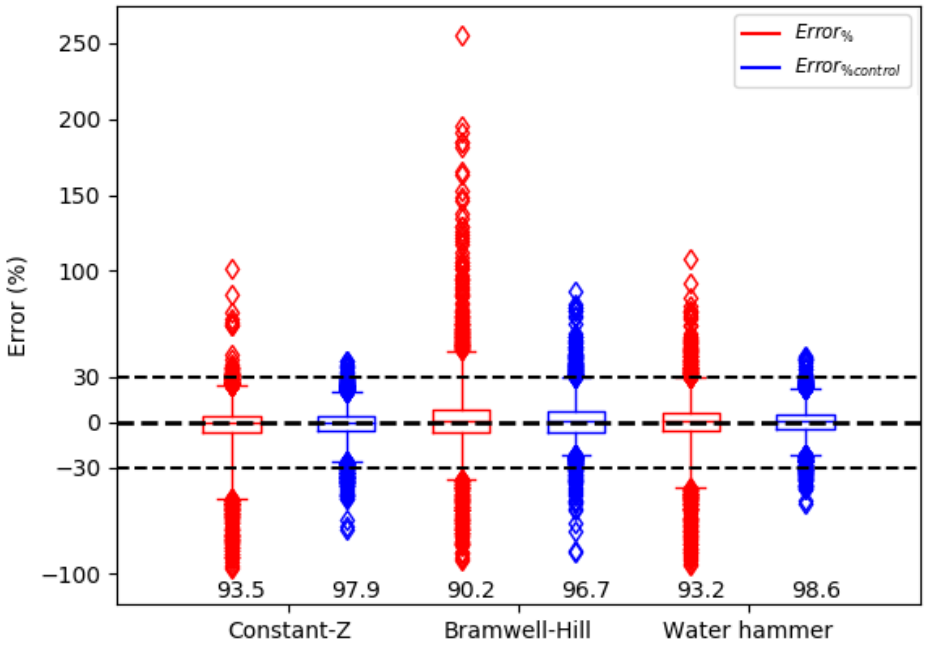

Figure 7: Box plot for $error_{\%}$ and $error_{\%control}$ for each method used to estimate Z, across all pigs and all interventions. Whiskers are at the 2.5th and 97.5th percentiles, with all errors outside these percentiles plotted individually. The values indicate the percentage of errors which fall within $\pm$ 30%".

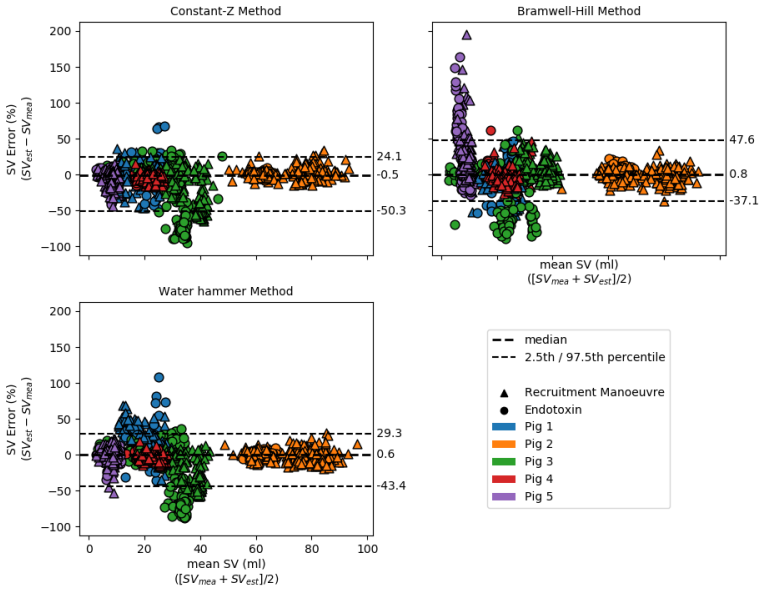

Figure 8: Bland-Altman analysis for SV percentage error ($error_{\%}$) for each method used to estimate Z. Median bias between measured and estimated SV are shown, as well as the 2.5th and 97.5th percentiles. For clarity, every 5th SV measurement is plotted, with none of 50 highest-error SV estimates for each stage omitted.

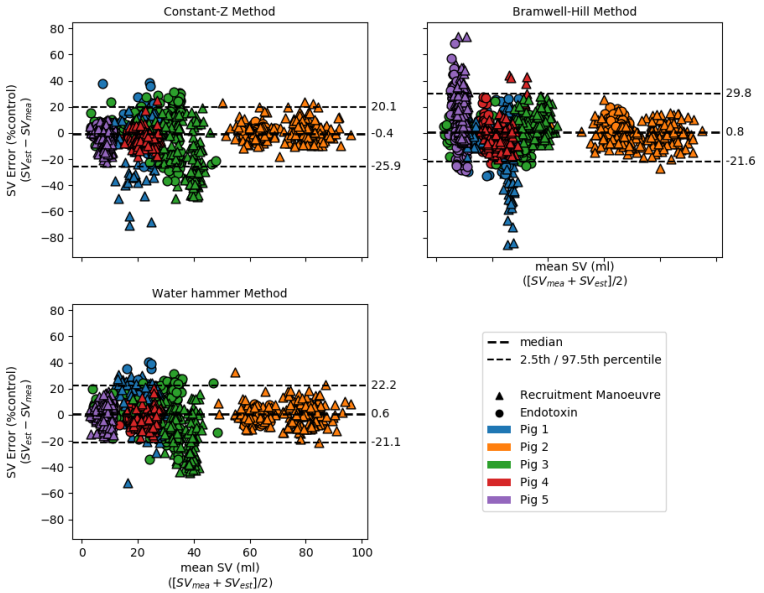

Figure 9: Bland-Altman analysis for SV $error_{\%control}$ for each method used to estimate Z. Median bias between measured and estimated SV are shown, as well as the 2.5th and 97.5th percentiles. For clarity, every 5th SV measurement is plotted, with none of 50 highest-error SV estimates for each stage omitted.

4. Discussion

4.1. Response to Interventions

The experimental protocol provided a range of SVs to test the model (SV ranges are given in Table 1). The endotoxin infusion led to circulatory failure in Pigs 1, 3, and 5, and for these pigs SV reduced to less than half of its baseline value during the endotoxin intervention (Table 1), providing examples of very severe hemodynamic instability.

4.2. Stroke volume estimation performance

The two best performing methods were the water hammer and constant-Z methods, with SV percentage error with a median bias and [(IQR); (2.5th, 97.5th percentile)] of 0.6% [(-4.9, 6.2); (-43.4%, 29.3%)] and -0.5% [(-6.1, 4.7); (-50.3%, +24.1%)], respectively. The Bramwell-Hill method performed poorly compared to the other methods with a median bias of 0.8% [(-6.5, 8.6); (-37.3%, +47.6%)]. The 95% range (97.5th - 2.5th percentile) for the Bramwell-Hill method was significantly larger than the other two methods (Table 3). The 95% range of the Constant-Z and water hammer methods was not significantly different, and the precision of these two methods is similar (Table 3).

The difference in median error was statistically significant for Constant-Z compared to both other methods, but not for Water hammer compared to Bramwell-Hill. However, the magnitude of the median difference, $< 1.8\%$ for

all cases (Table 3), is negligibly small, as compared to the the wide limits of agreement of current SV monitoring methods ($\approx \pm$ 45% [29]). Hence, although some methods had statistically significant differences in median error, clinically, the median differences are not appreciable, and in terms of bias these methods are clinically equivalent.

In general, the two best performing methods, water hammer and constant-Z, tracked changes in SV well (Figs B.1C - B.5C, Appendix B). The exception is Pig 3 for which these two methods overestimated the reduction in SV caused by both the recruitment manoeuvre and endotoxin infusion (Fig 5C). This overestimation occurred because the pig had a much larger reduction in pulse pressure at the femoral artery (P_{mea}), which is the input to the model, than the pressure reduction measured at the aortic arch (P_{ao}). For example, during the RM, P_{mea} PP dropped as low as 10 mmHg (compared to a baseline PP of 32 mmHg), whereas P_{ao} PP only dropped to 16 mmHg (compared to a baseline PP of 25 mmHg) (Table 1). This issue highlights a limitation of using the femoral artery to provide input pressures to the model. Specifically, while it is more clinically accessible, changes in arterial pressures at a distal location, such as the femoral artery, may not fully correspond to pressure changes in the proximal aorta.

The Bramwell-Hill method has high percentage errors for both events for Pig 5 (Table 2). In this pig, the Bramwell-Hill method did not capture the changes in SV (Fig B.5C, Appendix B) because changes in arterial pressures, and thus P_{ex} are offset by changes in Z_{bh} (Equation 3). Hence, for this Pig, this method of identifying Z led to predicting trends in SV very different

from trends in measured SV.

For this set of severe hemodynamic interventions, none of these methods meet the criteria reported by Critchley et al. [30] stating new CO monitoring techniques should have limits of agreement within +/- 30 % error, meaning 95% of errors should fall within this range. For the Constant-Z, Bramwell-Hill and water hammer methods, 94%, 90% and 93% of $error_{\%}$ fell within +/- 30 % error, respectively (Figs 7 and 8), which is just outside this criteria.

However, for extreme circulatory failure, such as for the endotoxin stage of Pig 3, pressures are so low precise measurement of SV / CO is not clinically relevant. Moreover, stroke volumes are very small, meaning errors of only a few mL can lead to very high percentage error. Using $error_{\%control}$ this numerical issue is ameliorated without simply eliminating extremely low SVs. For $error_{\%control}$ more than 95% of measurements fall within +/- 30 % error for all methods, as shown in Figs 7 and 9.

4.3. Pulse Wave Velocity

The addition of ΔPWV through the Bramwell-Hill method impaired model performance compared to the constant-Z method; the former had significantly wider limits of agreement than both the Constant-Z and water hammer methods (Table 2). The water hammer method had similar performance to the constant-Z method, with limits of agreement that were not significantly different (Table 2). Overall, neither the Bramwell-Hill nor water hammer methods appreciably improved accuracy or precision of SV estimation. Thus, the simpler constant-Z method, which does not require a PWV

measurement, is the most clinically promising.

The lack of improvement in model performance with incorporation of ΔPWV is likely because changes in PWV are already captured by changes in measured arterial pressures (Figs B.1- B.5B, Appendix B), due to the inherent pressure-dependence of PWV [31]. Thus it is possible that ΔPWV provides no additional information to the model beyond what is captured by the direct identification of parameter products ZC and RC from pulse contour analysis, as in [10].

4.4. Limitations

The 250 Hz sampling rate of the data means PTT was only resolvable to 4 ms. PTT had a range of 80 ms to 160 ms across all pigs, meaning only 21 distinct PTT values, and thus PWV values, were measured. Measurement of PTT / PWV would be improved with a higher sampling rate of the arterial pressure waveforms. However, it is unlikely a higher sampling rate and improved PWV measure would greatly change results, as the PTT resolution is able to capture trends in $1/PTT$ in response to interventions.

Additionally, two interventions were tested, respiratory recruitment manoeuvres and endotoxin. Under these conditions, changes in PWV did not greatly improve the SV estimation performance of the model. However, it is possible it may be important in other conditions, which should be investigated.

5. Conclusions

Non-additionally invasive methods for monitoring SV and CO need to reliably track hemodynamic changes during instability. Incorporating PWV using either the water hammer or Bramwell-Hill equation did not appreciably improve the ability of this pulse contour analysis model to capture SV changes during severe hemodynamic interventions. Thus, the windkessel model implementation using the constant-Z method remains the most promising approach. It thus remains a simple yet robust method, which could be implemented in a clinical setting without requiring any additional patient invasion, measurement of PWV, or new external device.

Acknowledgements

This study was supported with funding from the New Zealand Tertiary Education Commission Medtech CoRE and University of Canterbury Doctoral Scholarship. The funders had no role in study design, data collection and analysis, decision to publish or preparation of the manuscript.

References

[1] Y. Sakr, K. Reinhart, J.-L. Vincent, C. L. Sprung, R. Moreno, V. M. Ranieri, D. De Backer, D. Payen, Does dopamine administration in shock influence outcome? Results of the Sepsis Occurrence in Acutely Ill Patients (SOAP) Study*, Critical Care Medicine 34 (2006) 589–597.

[2] J. C. Orban, Y. Walrave, N. Mongardon, B. Allaouchiche, L. Argaud, F. Aubrun, G. Barjon, J.-M. Constantin, G. Dhonneur, J. Durand-Gasselin, H. Dupont, M. Genestal, C. Goguey, P. Goutorbe, B. Guidet, H. Hyvernat, S. Jaber, J.-Y. Lefrant, Y. Mallédant, J. Morel, A. Ouattara, N. Pichon, A.-M. Guérin Robardey, M. Sirodot, A. Theissen, S. Wiramus, L. Zieleskiewicz, M. Leone, C. Ichai, AzuRea, Causes and Characteristics of Death in Intensive Care Units, Anesthesiology 126 (2017) 882–889.

[3] D. A. Reuter, A. Kirchner, T. W. Felbinger, F. C. Weis, E. Kilger, P. Lamm, A. E. Goetz, Usefulness of left ventricular stroke volume variation to assess fluid responsiveness in patients with reduced cardiac function, Critical Care Medicine 31 (2003) 1399–1404.

[4] J. Huygh, Y. Peeters, J. Bernards, M. Malbrain, Hemodynamic monitoring in the critically ill: an overview of current cardiac output monitoring methods [version 1; peer review: 3 approved], F1000Research 5 (2016).

[5] T. Luecke, P. Pelosi, Clinical review: Positive end-expiratory pressure and cardiac output., Critical care (London, England) 9 (2005) 607–21.

[6] L. Busse, D. L. Davison, C. Junker, L. S. Chawla, Hemodynamic monitoring in the critical care environment., Advances in chronic kidney disease 20 (2013) 21–29.

[7] M. Cecconi, D. De Backer, M. Antonelli, R. Beale, J. Bakker, C. Hofer, R. Jaeschke, A. Mebazaa, M. R. Pinsky, J. Louis, T. Jean, L. Vincent, A. Rhodes, M. Cecconi, Á. A. Rhodes, D. De Backer, J. L. Vincent, M. Antonelli, R. Beale, J. Bakker, C. Hofer, R. Jaeschke, P. Diderot, P. Sorbonne, P. Cité, L. Aphp, M. R. Pinsky, J. L. Teboul, Consensus on circulatory shock and hemodynamic monitoring. Task force of the European Society of Intensive Care Medicine, Intensive Care Med 40 (2014) 1795–1815.

[8] J. Grensemann, Cardiac Output Monitoring by Pulse Contour Analysis, the Technical Basics of Less-Invasive Techniques, Frontiers in Medicine 5 (2018) 64.

[9] Y. Mehta, D. Arora, Newer methods of cardiac output monitoring., World journal of cardiology 6 (2014) 1022–1029.

[10] J. Balmer, C. G. Pretty, S. Davidson, T. Mehta-Wilson, T. Desaive, R. Smith, G. M. Shaw, J. G. Chase, Clinically applicable model-based method, for physiologically accurate flow waveform and stroke volume estimation, Computer Methods and Programs in Biomedicine 185 (2020) 105125.

[11] S. Laurent, J. Cockcroft, L. Van Bortel, P. Boutouyrie, C. Giannattasio, D. Hayoz, B. Pannier, C. Vlachopoulos, I. Wilkinson, H. Struijker-

Boudier, Expert consensus document on arterial stiffness: methodological issues and clinical applications on behalf of the European Network for Non-invasive Investigation of Large Arteries, European Heart Journal 27 (2006) 2588–2605.

[12] H. Fok, B. Jiang, B. Clapp, P. Chowienczyk, Regulation of Vascular Tone and Pulse Wave Velocity in Human Muscular Conduit Arteries Selective Effects of Nitric Oxide Donors to Dilate Muscular Arteries Relative to Resistance Vessels, Hypertension 60 (2012) 1220–1225.

[13] S. Kamoi, C. Pretty, J. Balmer, S. Davidson, A. Pironet, T. Desaive, G. M. Shaw, J. G. Chase, Improved pressure contour analysis for estimating cardiac stroke volume using pulse wave velocity measurement, BioMedical Engineering Online 16 (2017) 1–19.

[14] A. Lovas, T. Szakmány, Haemodynamic Effects of Lung Recruitment Manoeuvres, BioMed Research International 2015 (2015) 1–7.

[15] H. B. Nguyen, E. P. Rivers, F. M. Abrahamian, G. J. Moran, E. Abraham, S. Trzeciak, D. T. Huang, T. Osborn, D. Stevens, D. A. Talan, Emergency Department Sepsis Education Program and Strategies to Improve Survival (ED-SEPSIS) Working Group, Severe Sepsis and Septic Shock: Review of the Literature and Emergency Department Management Guidelines, Annals of Emergency Medicine 48 (2006) 28–54.

[16] M. Merx, C. Weber, Sepsis and the Heart, Circulation 116 (2007) 793–802.

[17] N. Westerhof, J.-W. Lankhaar, B. E. Westerhof, The arterial Windkessel, Medical & Biological Engineering & Computing 47 (2009) 131–141.

[18] N. Westerhof, N. Stergiopulos, M. I. M. Noble, Snapshots of Hemodynamics, Springer, New York, 2010.

[19] O. Frank, The basic shape of the arterial pulse. First treatise: Mathematical analysis, Journal of Molecular and Cellular Cardiology 22 (1990) 255–277.

[20] J.-J. Wang, A. B. O'Brien, N. G. Shrive, K. H. Parker, J. V. Tyberg, Time-domain representation of ventricular-arterial coupling as a windkessel and wave system, American Journal of Physiology-Heart and Circulatory Physiology 284 (2003) H1358–H1368.

[21] J. Balmer, C. Pretty, S. Davidson, T. Desaive, S. Kamoi, A. Pironet, P. Morimont, N. Janssen, B. Lambermont, G. M. Shaw, J. G. Chase, Pre-ejection period, the reason why the electrocardiogram Q-wave is an unreliable indicator of pulse wave initialization, Physiological Measurement 39 (2018) 095005.

[22] J. Balmer, R. Smith, C. G. Pretty, T. Desaive, G. M. Shaw, J. G. Chase, Accurate end systole detection in dicrotic notch-less arterial pressure waveforms, Journal of Clinical Monitoring and Computing (2020) 1–10.

[23] N. Westerhof, B. E. Westerhof, Waves and Windkessels reviewed, Artery Research 18 (2017) 102–111.

[24] A. Khir, K. Parker, Wave intensity in the ascending aorta: effects of arterial occlusion, Journal of Biomechanics 38 (2005) 647–655.

[25] J. C. Bramwell, A. V. Hill, The velocity of pulse wave in man, Proceedings of the Royal Society of London. Series B, Containing Papers of a Biological Character 93 (1922) 298–306.

[26] H. Motulsky, Intuitive biostatistics, Oxford University Press, 1995.

[27] D. G. Altman, J. M. Bland, Measurement in Medicine: The Analysis of Method Comparison Studies, The Statistician 32 (1983) 307.

[28] S. S. Mahmood, M. R. Pinsky, Heart-lung interactions during mechanical ventilation: the basics, Annals of Translational Medicine 6 (2018) 349–349.

[29] P. J. Peyton, S. W. Chong, Minimally invasive measurement of cardiac output during surgery and critical care, Anesthesiology 113 (2010) 1220–1235.

[30] L. A. Critchley, J. A. Critchley, A meta-analysis of studies using bias and precision statistics to compare cardiac output measurement techniques., Journal of clinical monitoring and computing 15 (1999) 85–91.

[31] B. Spronck, M. H. Heusinkveld, F. H. Vanmolkot, J. O. oodt, E. Hermeling, T. Delhaas, A. A. Kroon, K. D. Reesink, Pressure-dependence of arterial stiffness, Journal of Hypertension 33 (2015) 330–338.

A. Calculation of validation stroke volume metric (SV_{mea})

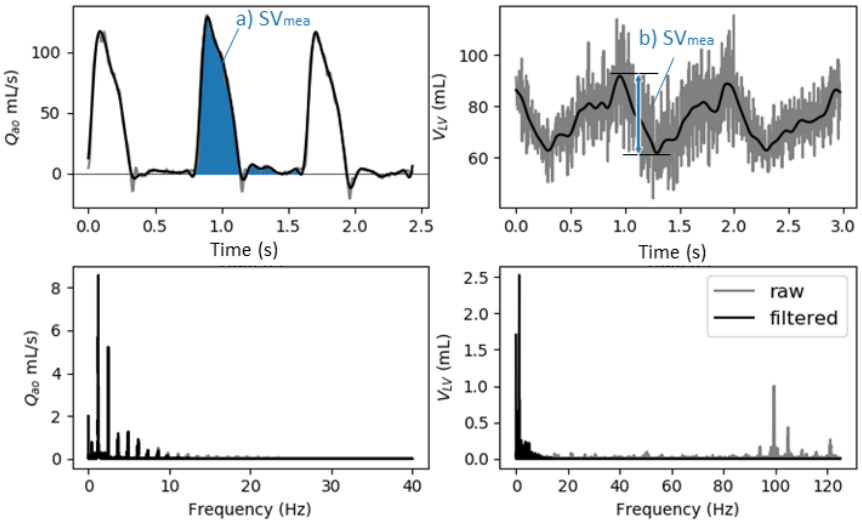

Figure A.1: Examples of Q_{ao} and V_{LV} raw and filtered signals in the time and frequency domains. SV_{mea} is calculated from filtered signals as a) the area under Q_{ao} for one beat, or b) the range of V_{LV} for one beat.

B. Additional Results

This appendix contains results Fig 5 for all pigs. The changes in arterial pressures, $1/PTT$, SV_{mea}, and SV_{est} in response to both of the interventions are shown in the following figures.

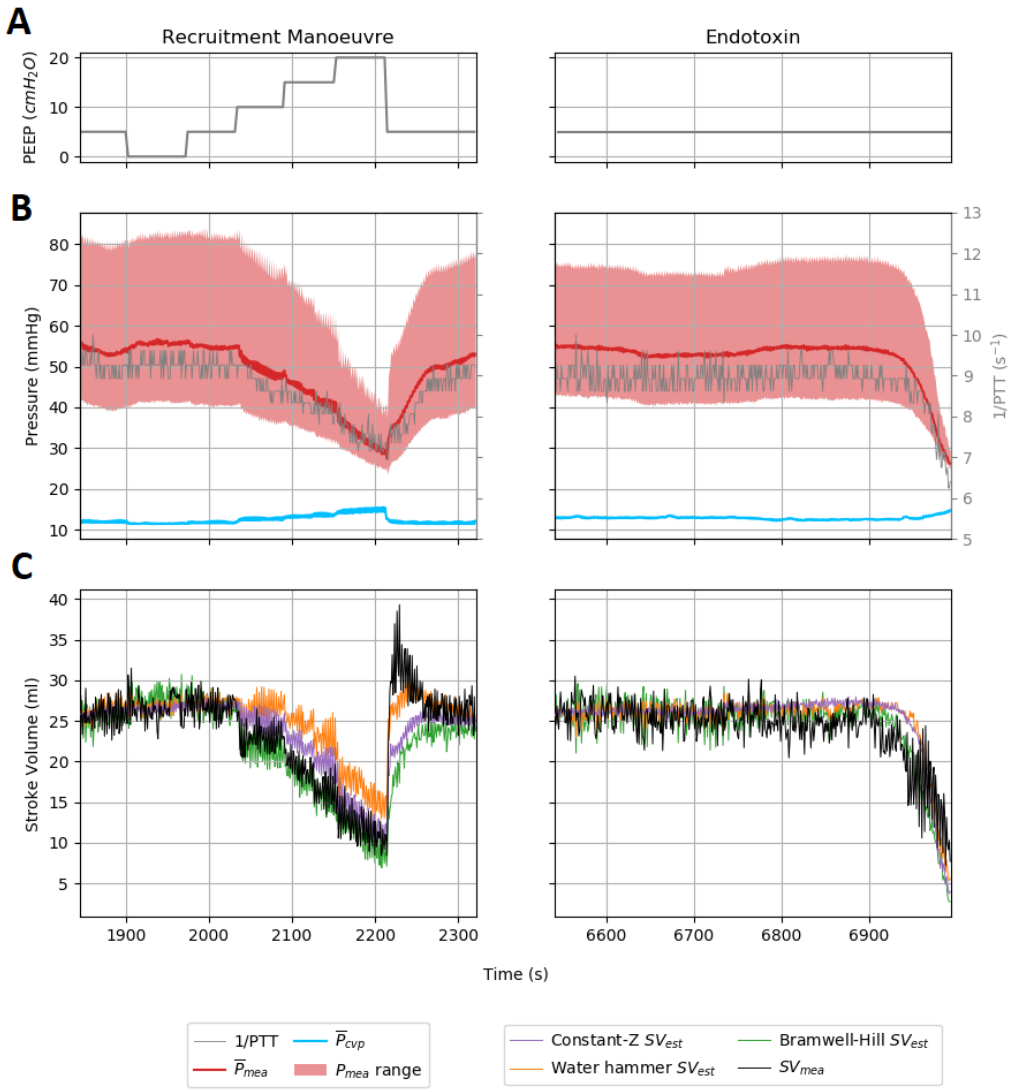

Figure B.1: Pig 1 signals for the full duration of both interventions. A) PEEP. For the RM intervention, PEEP is increased in steps to induce changes in SV and circulatory pressures. B) Model input signals: P_{cvp} is presented as mean pressure (calculated beat-wise) and P_{mea} is presented as beat-wise mean with the shaded area indicating range of pressures for each beat (foot and maximum pressure). $1/PTT$ is plotted on a secondary y-axis. C) SV_{mea} and modelled stroke volume, SV_{est}, for each method for estimating Z (Constant-Z, Water hammer, Bramwell-Hill)

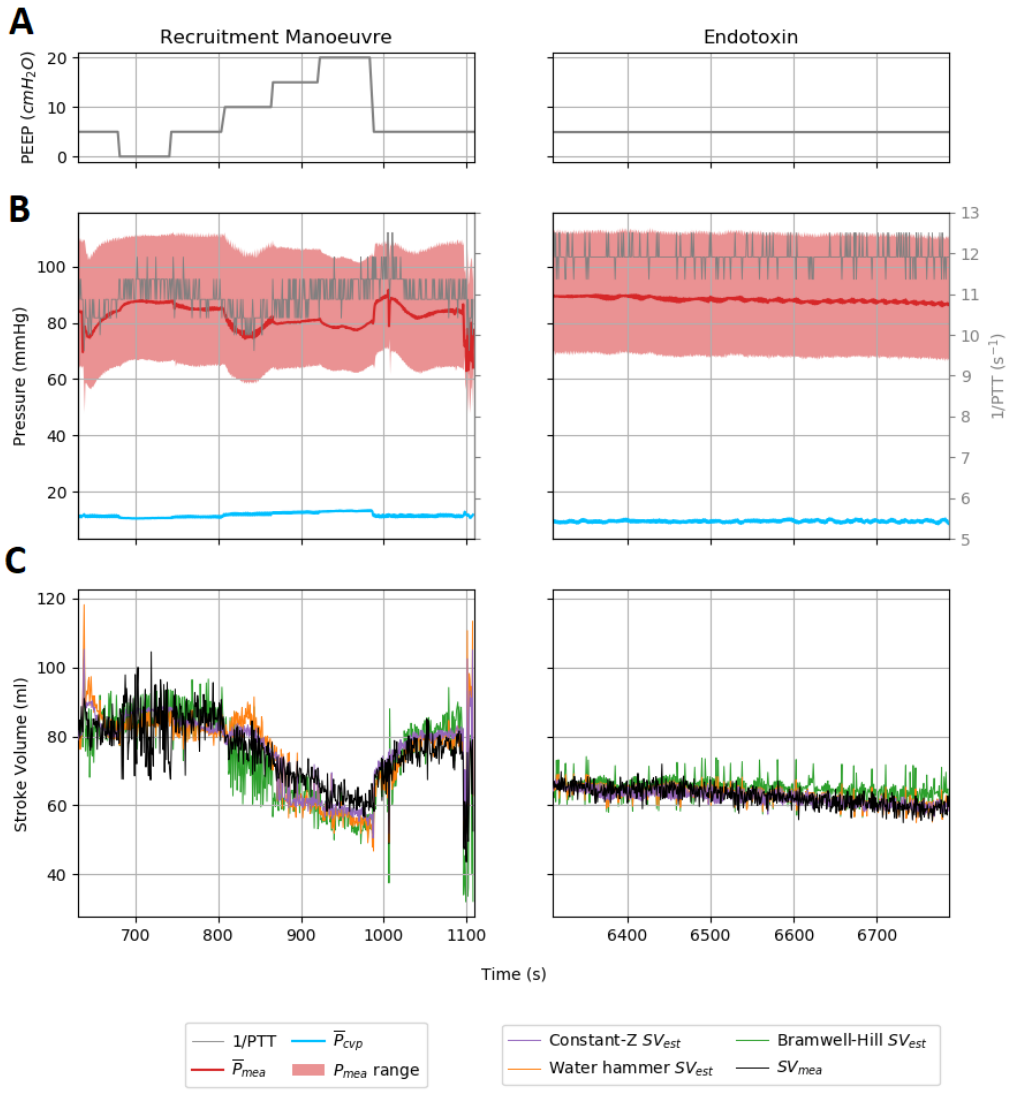

Figure B.2: Pig 2 signals for the full duration of both interventions. A) PEEP. For the RM intervention, PEEP is increased in steps to induce changes in SV and circulatory pressures. B) Model input signals: P_{cvp} is presented as mean pressure (calculated beat-wise) and P_{mea} is presented as beat-wise mean with the shaded area indicating range of pressures for each beat (foot and maximum pressure). $1/PTT$ is plotted on a secondary y-axis. C) SV_{mea} and modelled stroke volume, SV_{est}, for each method for estimating Z (Constant-Z, Water hammer, Bramwell-Hill).

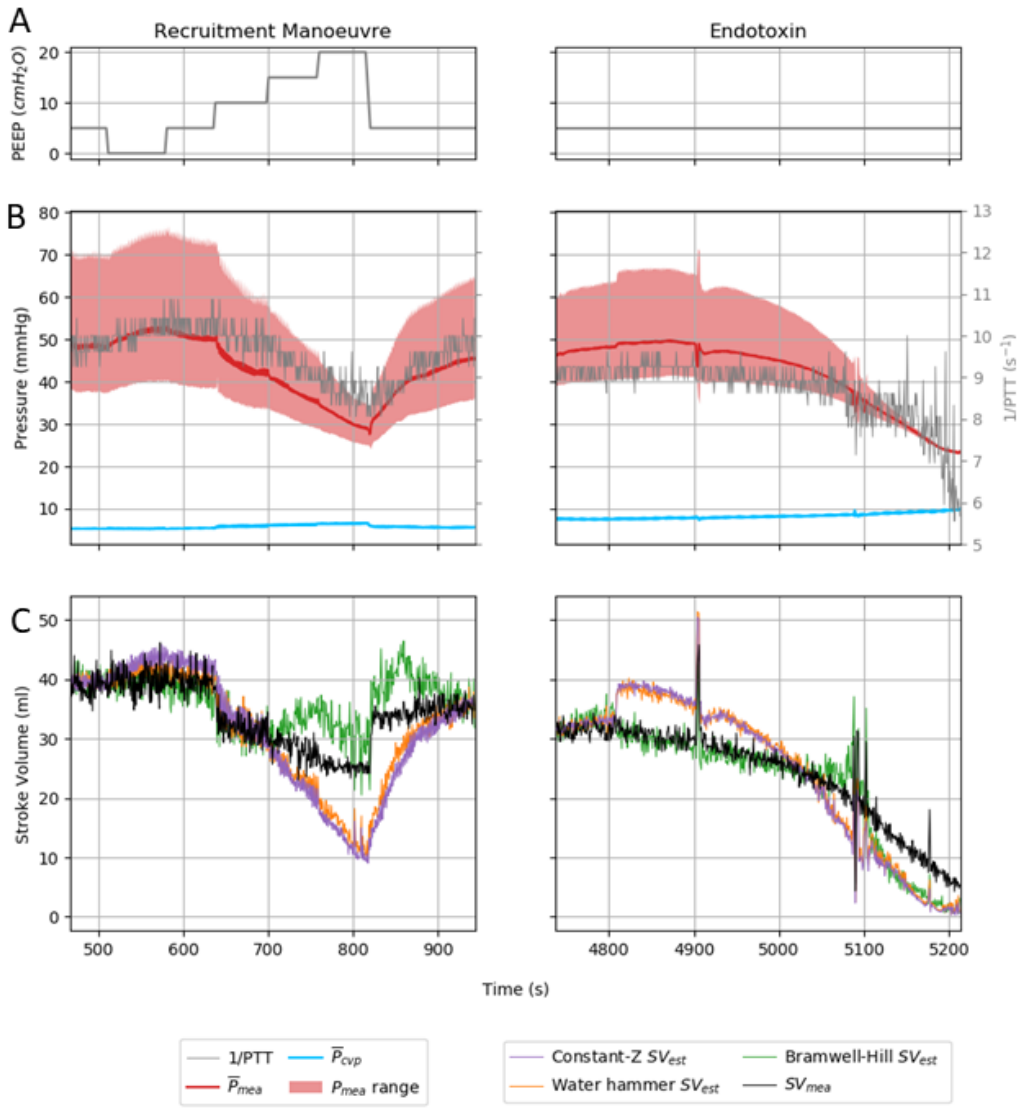

Figure B.3: Pig 3 signals for the full duration of both interventions. A) PEEP. For the RM intervention, PEEP is increased in steps to induce changes in SV and circulatory pressures. B) Model input signals: P_{cvp} is presented as mean pressure (calculated beat-wise) and P_{mea} is presented as beat-wise mean with the shaded area indicating range of pressures for each beat (foot and maximum pressure). $1/PTT$ is plotted on a secondary y-axis. C) SV_{mea} and modelled stroke volume, SV_{est}, for each method for estimating Z (Constant-Z, Water hammer, Bramwell-Hill)

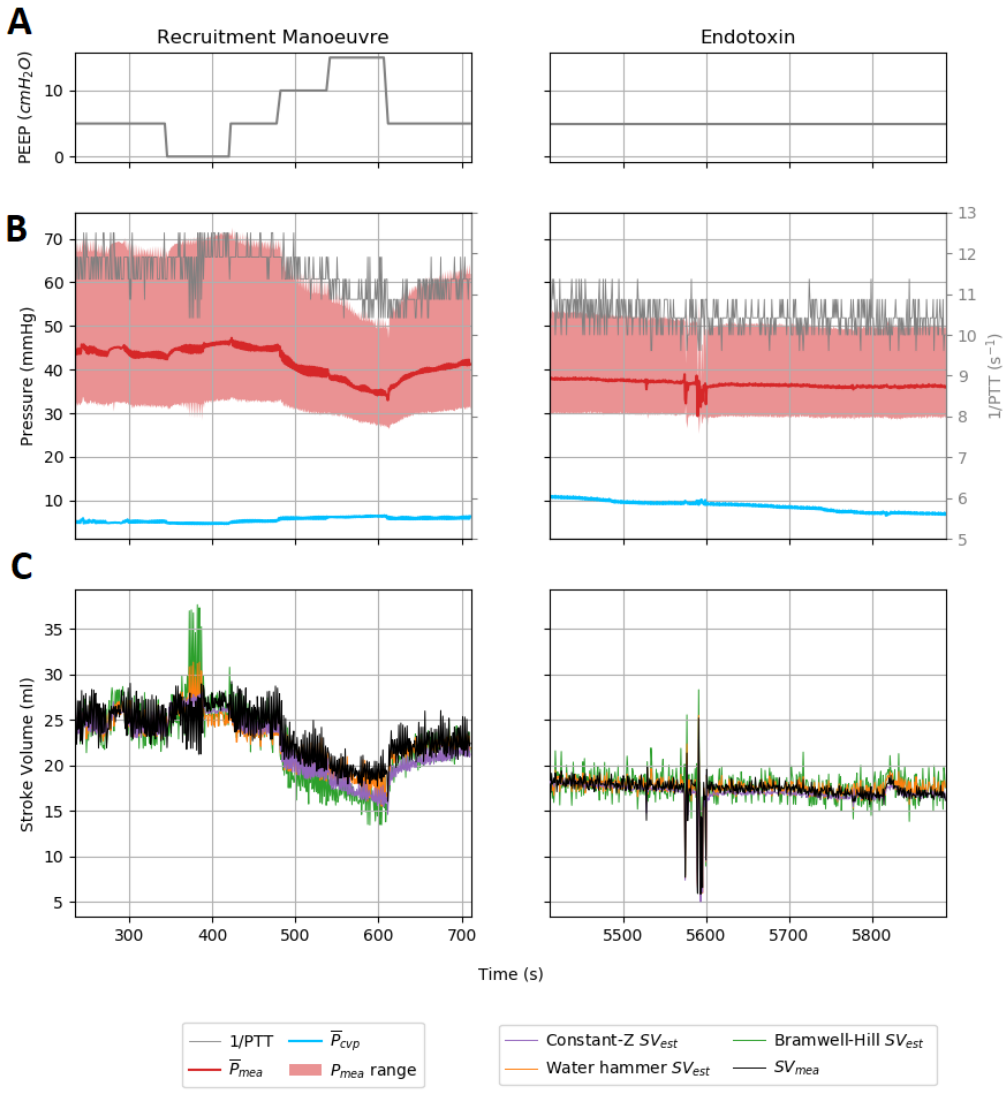

Figure B.4: Pig 4 Signals for the full duration of both interventions. A) PEEP. For the RM intervention, PEEP is increased in steps to induce changes in SV and circulatory pressures. B) Model input signals: P_{cvp} is presented as mean pressure (calculated beat-wise) and P_{mea} is presented as beat-wise mean with the shaded area indicating range of pressures for each beat (foot and maximum pressure). $1/PTT$ is plotted on a secondary y-axis. C) SV_{mea} and modelled stroke volume, SV_{est}, for each method for estimating Z (Constant-Z, Water hammer, Bramwell-Hill)

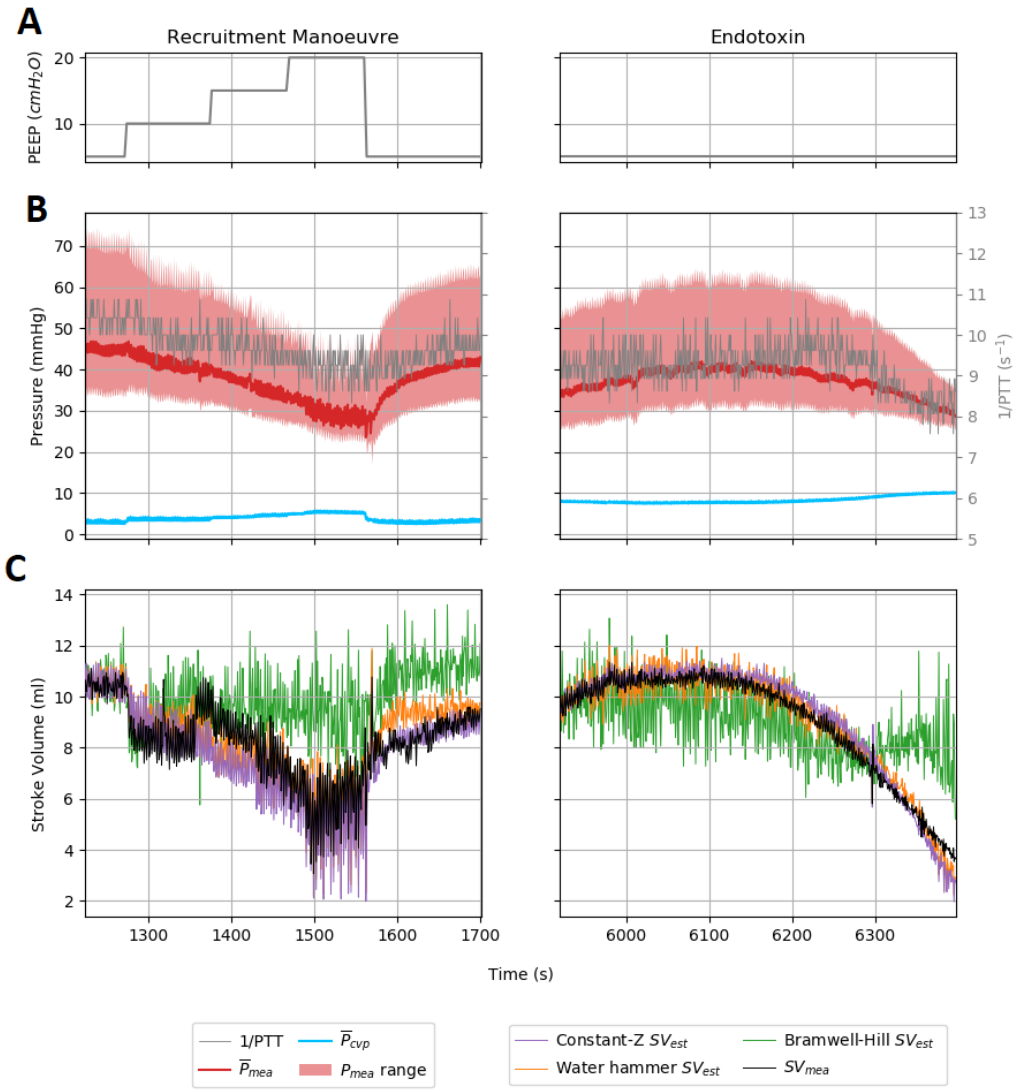

Figure B.5: Pig 5 Signals for the full duration of both interventions. A) PEEP. For the RM intervention, PEEP is increased in steps to induce changes in SV and circulatory pressures. B) Model input signals: P_{cvp} is presented as mean pressure (calculated beat-wise) and P_{mea} is presented as beat-wise mean with the shaded area indicating range of pressures for each beat (foot and maximum pressure). $1/PTT$ is plotted on a secondary y-axis. C) SV_{mea} and modelled stroke volume, SV_{est}, for each method for estimating Z (Constant-Z, Water hammer, Bramwell-Hill)